Article

Geometric Benchmarking of Metal Material Extrusion Technology: A Preliminary Study

Gabriele Locatelli ⓘ, Mariangela Quarto *ⓘ, Gianluca D'Urso ⓘ and Claudio Giardini ⓘ

Department of Management, Information and Production Engineering, University of Bergamo, Via Pasubio 7/b, 24044 Dalmine, BG, Italy; gabriele.locatelli@unibg.it (G.L.); gianluca.d-urso@unibg.it (G.D.); claudio.giardini@unibg.it (C.G.)
* Correspondence: mariangela.quarto@unibg.it

Abstract: Metal additive manufacturing technologies such as powder bed fusion (PBF) and direct energy deposition (DED) are experiencing fast development, due to the growing awareness of industries. However, high energy consumption, slow production processes, and high costs of both machines and feedstocks hamper their competitiveness, compared to conventional manufacturing techniques. Metal material extrusion (metal-MEX) can represent a cost- and energy-effective alternative for metal additive manufacturing. This article aims to assess the potential of such technology by addressing uncertainties related to product design and process stability through a preliminary geometric benchmarking study. The geometric tolerances and minimum achievable sizes of some simple geometries produced in 316L stainless steel were evaluated using geometric benchmark test artifacts (GBTAs). Process maps were also proposed to forecast the feasibility of achieving acceptable values of the investigated tolerances, based on the nominal dimensions of the features.

Keywords: additive manufacturing; metal 3D printing; metal-MEX; benchmarking; geometric tolerances

1. Introduction

Additive manufacturing (AM) is the general term used to address technologies that successfully join material layer upon layer to create physical objects as specified by 3D model data [1]. The progressive addition of material offers the possibility to overcome limitations typical of subtractive and plastic deformation processes, enabling great design freedom while avoiding the need for tooling and molds. This process optimizes resource usage by minimizing material waste, since the material is selectively added only where necessary [2]. Such findings are contributing to the widespread use of AM to produce functional components in many industrial fields, including aerospace [3], electronics [4], robotics [5], thermal management [6], automotive [7], and medical [8]. Particular interest is drawn by AM techniques, such as powder bed fusion (PBF) and direct energy deposition (DED), which are capable of selectively processing layers of metal powder and obtaining physical and mechanical properties comparable to those achieved through traditional technologies [9]. However, the competitiveness of such techniques is hindered by high energy consumption, slow build-up rates, and high costs of both the equipment and materials. Porosity defects formation during rapid solidification also represents a crucial challenge that deleteriously impacts material properties [10,11].

An economical alternative to the metal AM technologies mentioned above is represented by metal material extrusion (metal-MEX), also known as fused deposition modeling (FDM), since extrusion-based machines are cost-effective. Widely used for the production of polymeric parts, MEX has been adapted to metal components manufacturing by developing highly filled composite filaments. Such filaments have a complex multi-material formulation resulting from the homogenous mixture of sinterable metal powders and a polymeric binder system. The latter usually comprises a main binder component to

provide flowability to the filament, a backbone to supply shape retention, and additives to disperse the filler particles, thus preventing agglomeration and phase separation [12]. The content of metal particles in the filament strongly influences the properties of manufactured parts, resulting in reduced tensile strength and increased thermal conductivity [13,14]. In addition, the size, morphology, and composition of the particles also affect the mechanical and flow properties of the filament [15].

Due to the composite nature of the filament, metal parts are obtained only at the end of an indirect multi-step process, often referred to as shaping–debinding–sintering [16]. First, the extrusive shaping step is required to fabricate green parts using the MEX machine. Most of the binder system is then removed through catalytic [17], solvent, and/or thermal debinding [18]. The resulting highly porous brown parts (same volume, lower mass) are then subjected to a sintering treatment, performed below the melting temperature of the filler metal. The thermal cycle drives the formation of interparticle bonds, which grow, resulting in porosity reduction and near-total densification [12]. However, the impossibility of achieving full densification of sintered parts is responsible for developing anisotropic shrinkage, as proved by several studies [19,20]. Dimensional variations and distortions induced by thermal processing in metal-MEX ought to be compensated to ensure the design compliance of the parts, especially when manufacturing thin structures. The cost and energy required by post-printing treatments are subjected to the economy of scale by maximizing the number of components to be treated [21,22].

Performing geometrical and dimensional inspections is therefore essential to improve quality and to increase the confidence of industries in AM products [23]. Geometric capabilities, uncertainties, and limitations of AM processes can be quantitatively evaluated by fabricating and analyzing geometric benchmark test artifacts (GBTAs). Indeed, these artifacts are meant to be compared with design specifications to provide information on geometric dimensioning and tolerancing (GD&T) characteristics, dimensional accuracy, minimum feature size, repeatability, and surface finish [24].

After a critical review of existing works on the topic of tolerancing, it was observed that different studies already investigated, to different extents, both the geometric and dimensional tolerances of metal products realized through PBF processes [25–27], as well as parts obtained by traditional MEX of plastic filaments [28–30]. Rupal et al. [25] designed a benchmarking artifact with mating components to study the geometric and assemblability tolerancing of laser powder bed fusion (LPBF) using both the random field theory and thermo-mechanical simulations. The method proposed by the authors was then used to extract standardized GD&T quantifiers. Montero et al. [26] proposed a methodology for designing geometrical benchmarks for metal LPBF systems based on the designers' needs. A simple test artifact was created to experimentally validate the proposed methodology and outline an uncertainty map for relevant geometric characteristics using a relative coordinates system. Moshiri et al. [27] conducted an extensive benchmarking activity on several LPBF machines to understand the influence of the individual machine on the final quality of predesigned specimens and to assess the capabilities and limitations of the technology. Specifically, the performances of five machines operated by their respective manufacturers and two machines operated by end users were compared to investigate different aspects, including feature dimension, surface roughness, and repeatability. Cappellini et al. [28] used the design of the experiment to investigate the effects of layer thickness, printing speed, and number of contours on five geometric tolerances and the printing time of the MEX of the PLA plastic filament. Based on the results, the authors proposed a strategy to optimize process parameters to improve the accuracy and printing time of the MEX technology. Dantan et al. [29] proposed the combination of a simplified geometrical model with a modal representation of geometrical defects to predict the surface roughness and dimensional deviations of the MEX process. The working principle of this model was illustrated through a case study considering a simplified test artifact printed in PLA. The authors also proposed a geometrical simulation tool combining a Monte Carlo simulation and an optimization algorithm to assess the impacts of the geometrical deviations on an

assembly. Grgić et al. [30] proposed a methodology based on IT grades to improve the dimensional accuracy of parts printed through the MEX technique. Several hole and shaft assemblies were modeled as the arithmetic mean of the minimum and maximum diameter allowed by each tolerance zone between IT9 and IT14. The dimensions of the specimens were then evaluated through a noncontact measurement procedure, and the resulting roundness tolerances were determined.

To the best of the authors' knowledge, no study available in literature has ever been conducted to provide a geometrical or dimensional characterization of the metal-MEX technology. This paper addresses the existing gap in knowledge by initiating a comprehensive geometrical characterization study, with the primary goals of mitigating product design uncertainties and improving the technical feasibility of the metal-MEX process. A preliminary investigation was thus conducted by printing geometrical artifacts using a composite filament comprising 316L stainless steel powder to reproduce a variety of simple primitive shapes with varying dimensions. The analyzed features were then used to investigate the achievable geometrical tolerances with metal-MEX and concurrently determine the lower technological thresholds of the technology. This analysis included the definition of the minimum feasible sizes for such elementary features, thereby contributing valuable insights to the optimization of the metal-MEX process.

2. Materials and Methods

2.1. Artifacts Design and Fabrication

As per the feature-based methodology [23], the geometric tolerances were assessed through prismatic and cylindrical primitive features that simplify distinctive or characteristic parts of more complex workpieces. Thin wall and prismatic pillars were therefore chosen to evaluate perpendicularity, hollow cylinders were considered to assess coaxiality, and bridges were introduced to characterize the parallelism values through suspended horizontal beams. Based on the above considerations, five different GBTAs (Figure 1) were designed in agreement with the artifact decomposition proposed by ISO/ASTM 52902:2023 [31]. The fabrication of small, separate artifacts allowed for shorter build times, lower material consumption, and reduced distortion resulting from residual stresses [32].
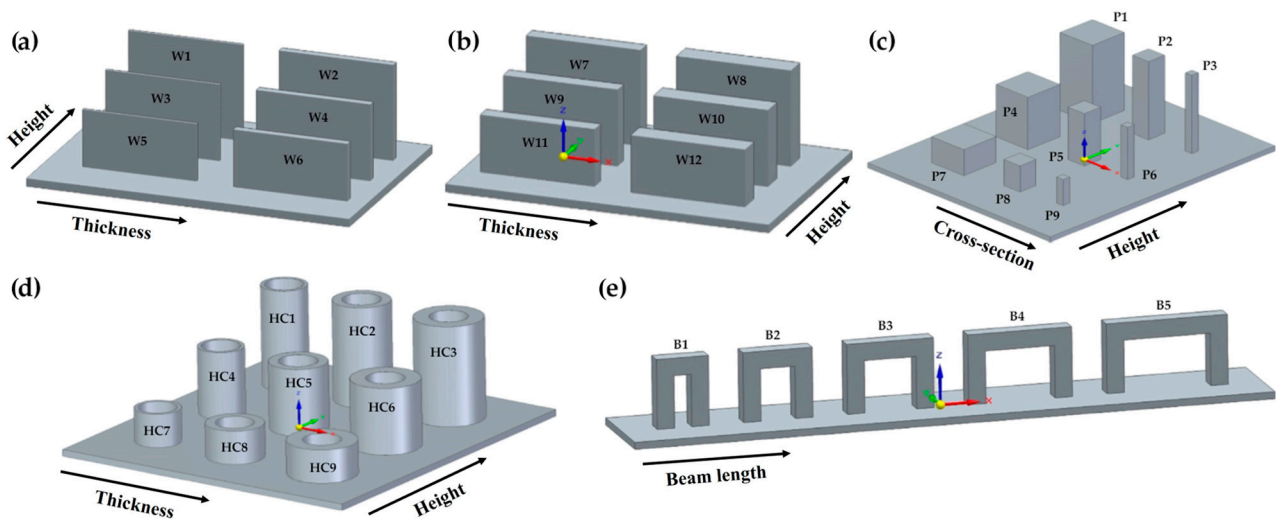
Figure 1. CAD geometries: (**a**) first thin walls GBTA; (**b**) second thin walls GBTA; (**c**) pillars GBTA; (**d**) hollow cylinders GBTA; (**e**) bridges GBTA.

The variable feature sizes included in each artifact shown in Figure 1 were chosen to consider the effect of scalability and to determine the minimum size achievable for each feature. In particular, the walls (Figure 1a,b) were characterized by heights of 15 mm, 20 mm, and 25 mm and thicknesses equal to 0.6 mm, 2 mm (Figure 1a), 4 mm, and 6 mm (Figure 1b), while the length was kept constant and equal to 30 mm. Figure 1c depicts pillars

characterized by heights of 10 mm, 20 mm, and 30 mm, while the square cross-sections were equal to 10×10 mm^2, 5×5 mm^2, and 2×2 mm^2. The nine hollow cylinders of Figure 1d had a constant inner diameter equal to 12 mm, while the external diameter increases were equal to 14 mm, 18 mm, and 22 mm. The heights were equal to 12 mm, 24 mm, and 36 mm. The last artifacts, reported in Figure 1e, were bridge structures whose thicknesses and heights were kept constant at 6 mm and 24 mm, while the length of the horizontal beam ranged from 6 mm to 30 mm, with a 6 mm interval. The height-to-thickness ratios (length-to-thickness for the bridges) of the designed features are summarized in Table 1.

Table 1. Nominal dimensional ratios of the designed features.

Geometry	Feature	Thickness (mm)	Height (mm)	Height-to-Thickness Ratios
Thin wall	W1	0.6	25	41.60
	W2	2	25	12.50
	W3	0.6	20	33.30
	W4	2	20	10.00
	W5	0.6	15	25.00
	W6	2	15	7.50
	W7	4	25	6.25
	W8	6	25	4.16
	W9	4	20	5.00
	W10	6	20	3.33
	W11	4	15	3.75
	W12	6	15	2.50
Pillar	P1	10	30	3.00
	P2	5	30	6.00
	P3	2	30	15.00
	P4	10	20	2.00
	P5	5	20	4.00
	P6	2	20	10.00
	P7	10	10	1.00
	P8	5	10	2.00
	P9	2	10	5.00
Hollow cylinder	HC1	1	36	36.00
	HC2	3	36	12.00
	HC3	5	36	7.20
	HC4	1	24	24.00
	HC5	3	24	8.00
	HC6	5	24	4.80
	HC7	1	12	12.00
	HC8	3	12	4.00
	HC9	5	12	2.40
Bridge	B1	6	6	1.00
	B2	6	12	2.00
	B3	6	18	3.00
	B4	6	24	4.00
	B5	6	30	5.00

2.2. Equipment and Material

All the proposed GBTAs were fabricated using an Ultrafuse 316L filament with a diameter of 2.85 mm, provided by BASF SE, Heidelberg, Germany. The filament could be handled safely and easily due to the AISI 316L powder (90 wt%) being immobilized in a binder matrix made up of polyoxymethylene (POM) and polyolefin (PO). Green parts were produced using an Ultimaker S5 MEX machine (Ultimaker, Utrecht, The Netherlands), whose direct drive extruder was equipped with a CC0.6 high wear resistance hardened steel nozzle (0.6 mm diameter) to avoid clogging and abrasion during extrusion. Support structures were introduced to sustain the beams of bridge features during printing. Such

supports were realized using BASF Ultrafuse Support Layer, a ceramic-based filament specifically developed to be used in combination with metal filaments and easily removable at the end of the shaping–debinding–sintering process. Figure 2 shows the printing equipment and the filament used for the experiments. All the proposed artifacts were realized according to the printing parameters suggested by the Ultrafuse user guidelines [33] and are summarized in Table 2.

Figure 2. Ultimaker 5S machine and BASF Ultrafuse 316L filament.

**Table 2.** Printing parameters for the Ultrafuse 316L filament.

Nozzle Temperature	Build Plate Temperature	Infill Type	Infill Density	Printing Speed	Layer Thickness
240 °C	100 °C	Line	100%	30 mm/s	0.2 mm

The green part was characterized by a composite material; specifically, the parts were composed of a polymeric matrix containing stainless steel powder. To obtain real metal parts (white part), the green parts must be subjected to debinding and sintering processes, which remove polymer components and consolidate the bonding of the powder grains. These treatments were conducted by an external company that applied the guidelines defined directly by BASF. The first treatment was the catalytic rebinding, and the thermal debinding process was performed at 393.15 K in an HNO_3 environment (98% concentration) to remove the main polymer content. The resulting brown parts were equal in volume to the initial green parts, but a loss of mass was experienced due to the decay of the polymer component. The sintering cycle, necessary for secondary binder removal and metal particle coalescence (white part), took place in an argon atmosphere and involved three thermal ramps. First, the temperature increased at a rate of 5 K/min from room temperature up to 873.15 K, which was held for 1 h. The temperature was then increased again at a rate of 5 K/min until it reached 1653.15 K. After being held for 3 h, the temperature decreased to room temperature through furnace cooling.

2.3. Geometric Tolerances Measurement and Evaluation

This characterization study investigated the perpendicularity, coaxiality, and parallelism tolerances achievable at the end of the metal-MEX process. The fabricated artifacts were measured using a Zeiss O-Inspect coordinate measuring machine (CMM) in both the

green state and the sintered state to determine the values of GD&T characteristics before and after the debinding and sintering treatments. The necessary profiles and elements of the artifacts were digitalized by automatic and continuous acquisition using the CMM touching probe. The measurements were digitally recorded by the metrology software Calypso 2022, which was then used to estimate the geometric tolerances of interest as deviations from the nominal CAD designs, which served as the reference standard (i.e., deviation equal to 0). Perpendicularity and parallelism tolerances were measured for each characteristic face of the respective feature using the base plates of the GBTAs as the reference datum (Figure 3). To provide a clear comparison across different geometries, a decision was made to select a single representative measure of geometric tolerance for each geometry. This approach aimed to maintain consistency and facilitate a uniform interpretation of the results. By identifying the tolerance measure that exhibited the maximum deviation from the nominal dimensions, a rigorous assessment of the geometrical specifications achievable through metal-MEX was ensured. Furthermore, by focusing on the most significant deviations from the nominal designs, the analysis provided valuable insights into the critical aspects of geometric performance in additive manufacturing.
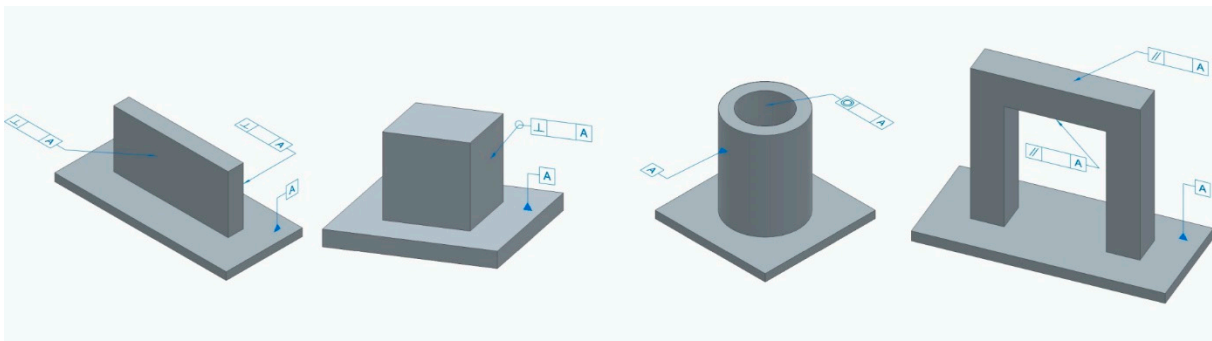
**Figure 3.** Tolerance surfaces and reference datum surfaces for the different features.

3. Results and Discussion

First of all, it is important to underline that following the debinding and sintering processes, the features of the GBTAs (Figure 4) underwent dimensional shrinkages equal to about 16% along the X and Y directions and about 20% along the growth direction, as already widely studied and reported in [20]. Subsequently, a comparison of the geometrical characteristics achieved by green parts and white parts was undertaken.
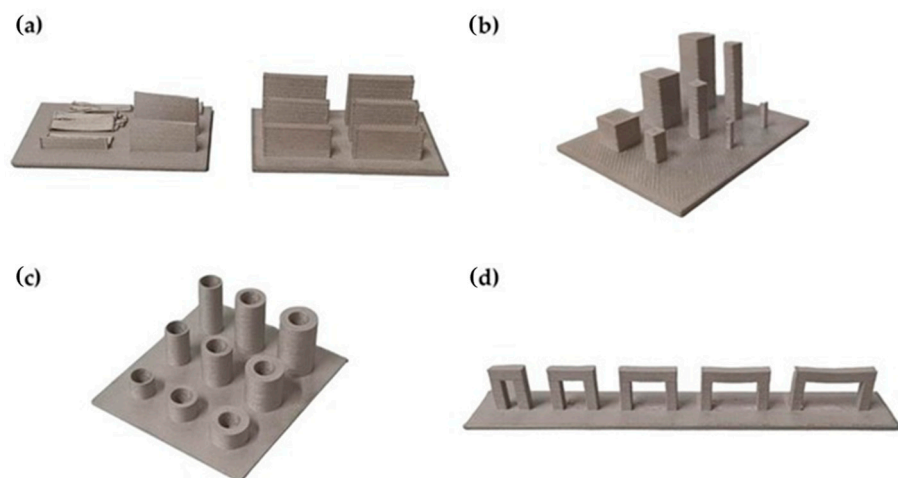
Figure 4. GBTAs in the white state resulting at the end of the metal-MEX process: (**a**) thin walls GBTA; (**b**) pillars GBTA; (**c**) hollow cylinders GBTA; (**d**) bridges GBTA.

A general overview of the geometrical characteristics analysis shows a worsening in perpendicularity and parallelism tolerances assessed through walls, pillars, and bridge features after debinding and sintering treatments, as depicted in Figure 5a, Figure 5b, and Figure 5d, respectively. Notably, a clear trend can be observed for the parallelism of the beams, which exhibits an exponential increase with beam length in the white state. In contrast, Figure 5c shows that coaxiality exhibits an opposite trend, compared to the previous tolerances, with green-part hollow cylinders displaying poorer coaxiality values compared to the final white parts.
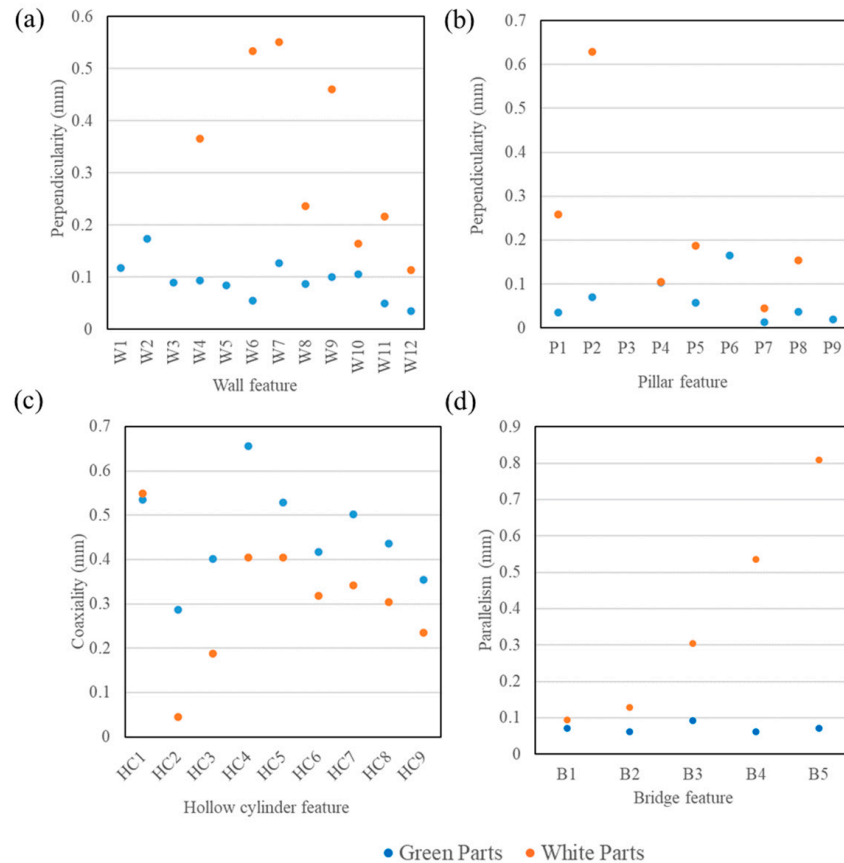
Figure 5. Comparison of geometrical characteristics of the green parts and white parts: (**a**) perpendicularity of wall features; (**b**) perpendicularity of pillar features; (**c**) coaxiality of hollow cylinder features; (**d**) parallelism of bridge features.

The acquired results were also leveraged to develop quantitative maps (Figure 6) that offer a comprehensive understanding of how variations in feature dimensions impacted the quality and consistency of the parts manufactured through the metal-MEX process. These maps delineate the reliable operating range of the technology and underline deviations from the nominal geometry of the studied characteristics. Through the systematic analysis of the relationships between feature dimensions and geometric characteristics, these maps offer insights into the optimal dimensional ratio where the metal-MEX process proves most reliable. This type of outline can facilitate the establishment of guidelines to help manufacturers and engineers in the design and fabrication of components within specified ranges, ensuring resulting geometrical characteristics that meet the desired standards. Thus, these maps serve as invaluable tools for process design, enabling practitioners to ascertain the limits and constraints within which the metal-MEX process consistently delivers reliable and high-quality results. The maps also provide minimum achievable feature sizes. Specifically, the results show that the minimum achievable height-to-thickness or length-to-thickness ratios not resulting in collapse are equal to 2.50 (element W12), 1

(element P7), 2.40 (element HC9), and 1 (element B1) for thin walls, prismatic pillars, hollow cylinders, and bridges, respectively.
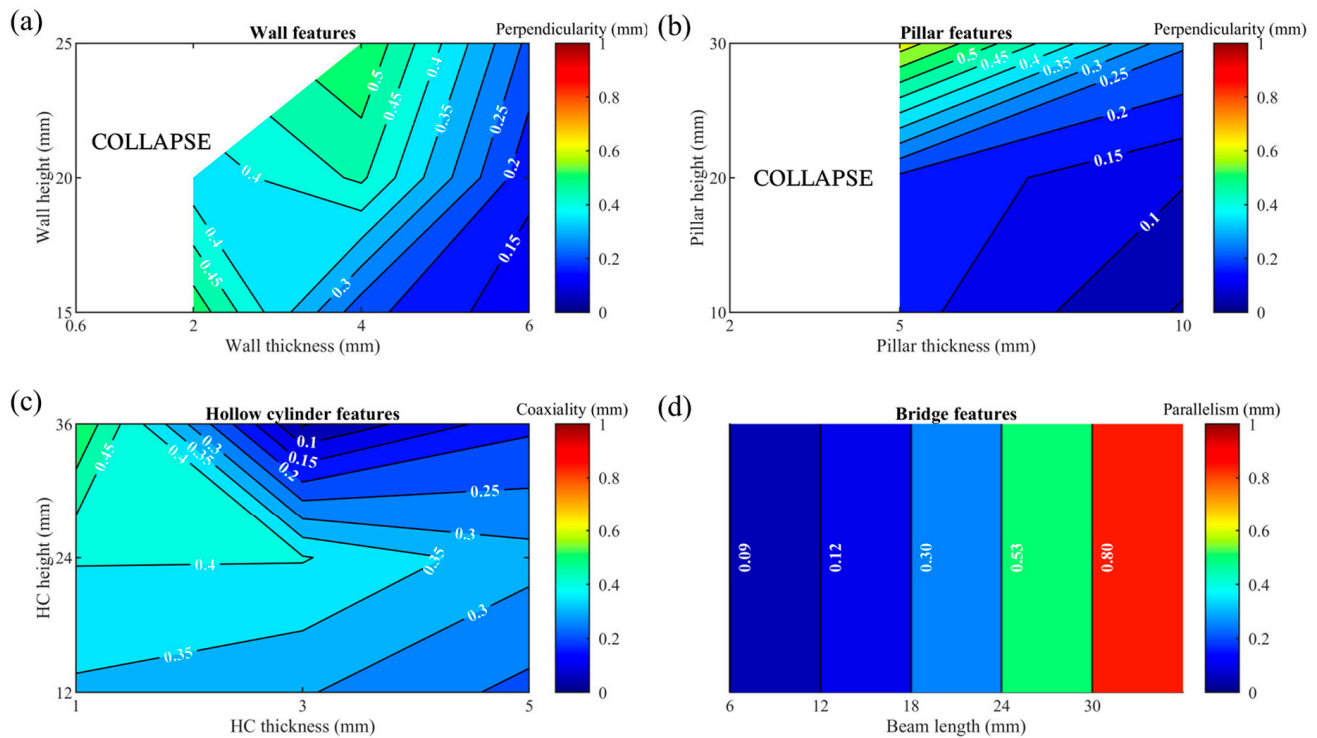

Figure 6. Maps for white-state geometric tolerances achievable with metal-MEX: (**a**) perpendicularity of wall features; (**b**) perpendicularity of pillar features; (**c**) coaxiality of hollow cylinder features; (**d**) parallelism of bridge features.

As expected, finer perpendicularity tolerances can be achieved for both wall and pillar elements by increasing the thickness and reducing the height, as depicted in Figures 6a and 6b, respectively. Conversely, excessively increasing the height-to-thickness ratios of the features undermines the stability of the brown parts and leads to structural distortion or collapse, due to the cumulative effects of debinding and sintering, which, in turn, negatively affect the tolerance values. Indeed, Figure 7 depicts how the post-printing treatments resulted in the development of residual stresses within the structures, which ultimately led to the collapse of the thinnest wall and pillar features (W1, W2, W3, W5, P6, and P9) and the torsional deformation of other elements in the white state. On the other hand, it must also be noted that the fabrication of feature P3 failed directly at the printing stage, most likely due to its combination of the highest height and lowest thickness values among pillar features. The technical guidelines provided by the producer of the Ultimaker 316L filament suggest that feature distortion and collapse during debinding and sintering can be prevented by limiting the nominal height-to-width ratio below 3 and 6 for pillars and thin walls, respectively [33]. However, it is noteworthy that our study observed discrepancies with these guidelines. While collapse and distortion were indeed observed when the suggested ratios were exceeded, contrary to expectations, such problems were also encountered below these values. In particular, no dimensional ratio lower than 6 prevented distortions in thin walls, while only a height-to-thickness ratio equal to 1 proved enough to achieve an undistorted pillar feature. Bridges represent the most critical structures in terms of deformations occurring at the end of the metal-MEX production process. Acceptable parallelism values were indeed achieved only by features B1 and B2, whose horizontal beams were shorter than 18 mm, as depicted by the map in Figure 6d. Despite ceramic-based support structures being included to sustain the structures during debinding and sintering, further lengthening the beam resulted in the prominent inflection of elements B3,

B4, and B5, as shown in Figure 7. However, the Ultimaker guidelines do not provide any effective ratio to prevent the collapse or distortion of horizontally suspended geometries like the beams of bridge features. Based on the results of our study, it is thus not advisable to exceed a nominal length-to-width ratio of 2 when fabricating bridge features with ceramic-based supports through metal-MEX. On the contrary, hollow cylinders appear instead to be characterized by a more stable structure, since no collapse was observed throughout the production process, despite height-to-thickness ratios ranging from as low as 2.40 to as high as 36. Furthermore, the map in Figure 6c shows that finer coaxiality can be achieved not only through thicker and shorter features but also by concurrently increasing both the height and the thickness of the hollow cylinder, thus suggesting that thickness plays a more significant role in achieving structural integrity for these geometries. Interestingly, unsupported hollow protruding geometries are not addressed in the guidelines; thus, no insight or optimal limit ratio is available for comparison.
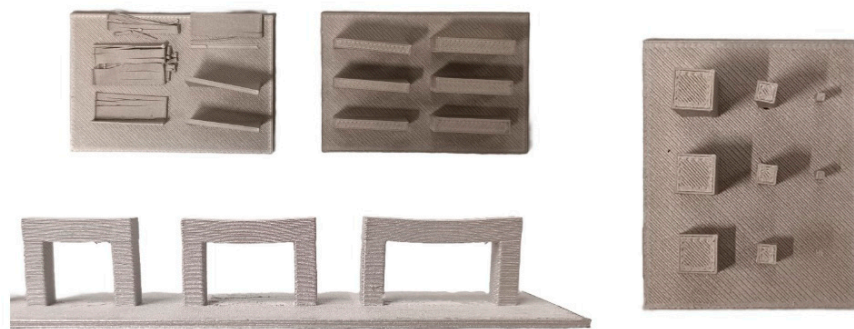

Figure 7. Details of collapsed and distorted features of white parts.

It is crucial to highlight that the success of the printing phase and the entire process is closely tied to the geometry of the nozzle, especially its diameter, as it affects the number of adjacent depositions in each layer. The nozzle's diameter also determines the width of the extruded filament, thereby impacting the minimum size of the features. Therefore, achieving a precise replication of the geometry may be at risk if a feature's dimension is smaller than the nozzle's diameter. This problem emphasizes how the nozzle's diameter might affect the achievable aspect ratio. In the metal-MEX process, as the layer height increases, there might be a restriction on the aspect ratio of features, due to the expansion of the deposited material strand caused by a larger nozzle diameter. Consequently, if the aspect ratio becomes too high, layers could become unstable or fail to adhere correctly. Therefore, smaller nozzles would allow for finer details and smaller features to be printed but might limit achievable aspect ratios due to increased layer width compared to height. On the other hand, larger nozzles would enable faster printing and higher aspect ratios but might sacrifice detail and resolution for smaller features.

It is then clear that achieving dimensional accuracy requires a careful balance of nozzle diameter, layer height, print speed, and level of detail suited to a particular project. The graphs in Figure 6 show that no positive results were achieved for features with thicknesses closely related to the 0.6 mm nozzle diameter used in this study. However, it is important to note that the results should be adapted for smaller nozzle diameters. A further elaboration of these graphs can be performed to clarify the relationship between the smallest feasible size of the basic features and the aspect ratio between the feature's thickness and the nozzle's diameter. Introducing the ratio between the feature's thickness and the nozzle's diameter in the previous maps, as illustrated in Figure 8, enables the generalization of the results. This inclusion allows for a comprehensive examination of how the nozzle might impact the quality of replicated features. Notably, Figure 8a allows for the assumption that when the wall thickness matches the diameter of the nozzle, structural failure consistently occurs, regardless of the selected height. However, increasing the feature–nozzle ratio to a minimum value of 3.33 might prevent collapse, particularly if the feature's height

does not exceed 20 mm. Further increasing the ratio could possibly diminish the adverse impact of height restrictions, thus enabling the production of taller, slender walls. It is also observed that achieving heightened precision in terms of perpendicularity might necessitate that wall thickness be ten times greater than the nozzle diameter. A similar pattern is observed for cuboidal pillars, as depicted in Figure 8b. In this case, a thickness exceeding 8.33 times the nozzle diameter might be imperative to prevent structural failure throughout all stages, from printing to sintering. Additionally, it might prove beneficial to limit pillar height while simultaneously augmenting the feature–nozzle ratio up to 16.66 to enhance the perpendicularity values of the features. Hollow cylindrical features can be manufactured without experiencing collapse within a feature–nozzle ratio range of 1.66 to 8.33, as depicted in Figure 8c. Even for such geometries, increasing the ratio of feature thickness to nozzle diameter might enhance the fabrication of more accurate reproductions of coaxially aligned features. A similar elaboration of the map devised for bridge structures could not be provided, as the length of the beams was the only dimension to be varied in this study. The number of strands deposited for each layer would indeed remain the same for differently sized nozzles. However, it is still possible to assume that an accurate reproduction of bridge features with a thickness ten times higher than the nozzle's diameter might be achieved only when limiting the length of the beam below 18 mm, even if support structures are also kept in place during debinding and sintering.
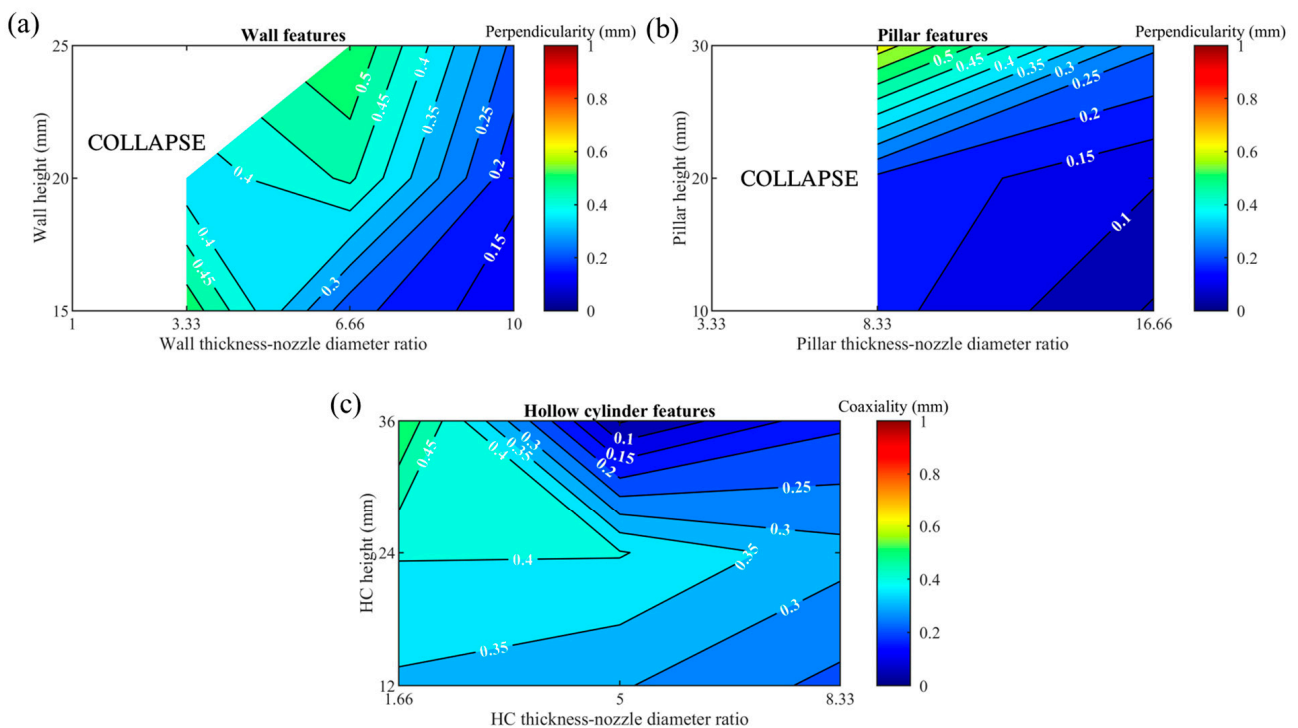
Figure 8. Maps for white-state geometric tolerances considering the ratio between the feature's thickness and the nozzle's diameter: (**a**) wall features; (**b**) pillar features; (**c**) hollow cylinder features.

The generalization of the results suggests the assumption that an effective approach to prevent structural collapse and to enhance geometrical precision is to produce geometric features with a thickness largely exceeding the diameter of the extrusion nozzle. However, the validation of such an assumption requires further experiments to be performed.

Increasing this ratio leads to the deposition of a greater number of material strands per layer, thereby enhancing interlayer adhesion. Ensuring strong material adhesion during printing is crucial for preserving structural integrity during later stages of the metal-MEX process, particularly in the brown state, where metal particles have not yet undergone sintering and bonding.

4. Conclusions

Metal-MEX represents a cheaper alternative to powder bed fusion and direct energy deposition for the additive manufacturing of metals. However, the quality of the components still needs to be assessed in terms of geometrical performances to understand how the debinding and sintering treatments influence the achievable geometric characteristics. This work presents a preliminary geometrical characterization of 316L stainless steel geometric benchmark test artifacts produced using metal-MEX technology. The analyzed features were chosen to investigate geometric tolerances after both the printing process and the debinding and sintering treatments required to obtain dense metal parts.

Findings limited to the analyzed range of nominal characteristic dimensions revealed that the residual stresses induced by debinding and sintering ultimately affected the investigated geometrical tolerances. In general, degradations in perpendicularity and parallelism tolerances were observed in the white state. Notably, parallelism exhibited an exponential increase with the length of the beam in the white state. On the contrary, improvements were observed in the measures of coaxiality acquired through hollow cylindrical features. The results of this study identified that the metal-MEX technology can be used to fabricate 316L stainless steel complex parts composed of primitive features. It was also determined that the dimensional ratio of the features influences the feasibility of the process: over specific values, the white parts cannot be obtained, due to the collapse or distortion resulting from post-printing treatments. However, discrepancies with the guidelines provided by the producer of the filament were observed, as collapse and distortion were encountered both above and below the height-to-thickness ratios suggested for both thin walls and pillars. A general overview of the aspect ratio behavior was obtained and described by maps, where it was possible to derive the assumption that employing smaller nozzles, compared to the printed feature, might noticeably reduce the risk of structural collapse and enable the fabrication of geometrical reproductions that are more accurate in terms of geometrical tolerances. This represents a starting point for further research that should be dedicated to a deeper comprehension of how layer density, infill strategy, and residual stresses affect part distortion throughout the entire manufacturing process.

References

1. *ISO/ASTM 52900:2021*; Additive Manufacturing—General Principles—Fundamentals and Vocabulary. International Organization for Standardization: Geneva, Switzerland, 2021.
2. Rane, K.; Strano, M. A Comprehensive Review of Extrusion-Based Additive Manufacturing Processes for Rapid Production of Metallic and Ceramic Parts. *Adv. Manuf.* **2019**, *7*, 155–173. [CrossRef]
3. Khorasani, M.; Ghasemi, A.; Rolfe, B.; Gibson, I. Additive Manufacturing a Powerful Tool for the Aerospace Industry. *Rapid Prototyp. J.* **2022**, *28*, 87–100. [CrossRef]
4. Lu, B.-H.; Lan, H.-B.; Liu, H.-Z. Additive Manufacturing Frontier: 3D Printing Electronics. *Opto-Electron. Adv.* **2018**, *1*, 17000401–17000410. [CrossRef]
5. Gul, J.Z.; Sajid, M.; Rehman, M.M.; Siddiqui, G.U.; Shah, I.; Kim, K.-H.; Lee, J.-W.; Choi, K.H. 3D Printing for Soft Robotics—A Review. *Sci. Technol. Adv. Mater.* **2018**, *19*, 243–262. [CrossRef]
6. Jafari, D.; Wits, W.W. The Utilization of Selective Laser Melting Technology on Heat Transfer Devices for Thermal Energy Conversion Applications: A Review. *Renew. Sustain. Energy Rev.* **2018**, *91*, 420–442. [CrossRef]
7. Elakkad, A.S. 3D Technology in the Automotive Industry. *Int. J. Eng. Res. Technol.* **2019**, *8*, 248–251. [CrossRef]

8. Yan, Q.; Dong, H.; Su, J.; Han, J.; Song, B.; Wei, Q.; Shi, Y. A Review of 3D Printing Technology for Medical Applications. *Engineering* **2018**, *4*, 729–742. [CrossRef]

9. Frazier, W.E. Metal Additive Manufacturing: A Review. *J. Mater. Eng. Perform.* **2014**, *23*, 1917–1928. [CrossRef]

10. Laleh, M.; Hughes, A.E.; Yang, S.; Wang, J.; Li, J.; Glenn, A.M.; Xu, W.; Tan, M.Y. A critical insight into lack-of-fusion pore structures in additively manufactured stainless steel. *Addit. Manuf.* **2021**, *38*, 101762. [CrossRef]

11. Du, C.; Zhao, Y.; Jiang, J.; Wang, Q.; Wang, H.; Li, N.; Sun, J. Pore defects in Laser Powder Bed Fusion: Formation mechanism, control method, and perspectives. *J. Alloys Compd.* **2023**, *944*, 169215. [CrossRef]

12. Gonzlez-Gutirrez, J.; Beulke, G.; Emri, I. Powder Injection Molding of Metal and Ceramic Parts. In *Some Critical Issues for Injection Molding*; InTech: London, UK, 2012.

13. Hwang, S.; Reyes, E.I.; Moon, K.; Rumpf, R.C.; Kim, N.S. Thermo-Mechanical Characterization of Metal/Polymer Composite Filaments and Printing Parameter Study for Fused Deposition Modeling in the 3D Printing Process. *J. Electron. Mater.* **2015**, *44*, 771–777. [CrossRef]

14. Carminati, M.; Quarto, M.; D'Urso, G.; Giardini, C.; Maccarini, G. Mechanical Characterization of AISI 316L Samples Printed Using Material Extrusion. *Appl. Sci.* **2022**, *12*, 1433. [CrossRef]

15. Wu, G.; Langrana, N.A.; Sadanji, R.; Danforth, S. Solid Freeform Fabrication of Metal Components Using Fused Deposition of Metals. *Mater. Des.* **2002**, *23*, 97–105. [CrossRef]

16. Gonzalez-Gutierrez, J.; Cano, S.; Schuschnigg, S.; Kukla, C.; Sapkota, J.; Holzer, C. Additive Manufacturing of Metallic and Ceramic Components by the Material Extrusion of Highly-Filled Polymers: A Review and Future Perspectives. *Materials* **2018**, *11*, 840. [CrossRef] [PubMed]

17. Raza, M.R.; Ahmad, F.; Muhamad, N.; Sulong, A.B.; Omar, M.A.; Akhtar, M.N.; Aslam, M.; Sherazi, I. Effects of Debinding and Sintering Atmosphere on Properties and Corrosion Resistance of Powder Injection Molded 316 L—Stainless Steel. *Sains Malays.* **2017**, *46*, 285–293. [CrossRef]

18. Liu, B.; Wang, Y.; Lin, Z.; Zhang, T. Creating Metal Parts by Fused Deposition Modeling and Sintering. *Mater. Lett.* **2020**, *263*, 127252. [CrossRef]

19. Kurose, T.; Abe, Y.; Santos, M.V.A.; Kanaya, Y.; Ishigami, A.; Tanaka, S.; Ito, H. Influence of the Layer Directions on the Properties of 316L Stainless Steel Parts Fabricated through Fused Deposition of Metals. *Materials* **2020**, *13*, 2493. [CrossRef] [PubMed]

20. Quarto, M.; Carminati, M.; D'Urso, G. Density and Shrinkage Evaluation of AISI 316L Parts Printed via FDM Process. *Mater. Manuf. Process.* **2021**, *36*, 1535–1543. [CrossRef]

21. Quarto, M. An Empirical Method for Forecasting Energy Consumption in Material Extrusion. *Int. J. Adv. Manuf. Technol.* **2023**, *127*, 2911–2920. [CrossRef]

22. Quarto, M.; Giardini, C. Additive Manufacturing of Metal Filament: When It Can Replace Metal Injection Moulding. *Progress. Addit. Manuf.* **2023**, *8*, 561–570. [CrossRef]

23. Rivas Santos, V.M.; Thompson, A.; Sims-Waterhouse, D.; Maskery, I.; Woolliams, P.; Leach, R. Design and Characterisation of an Additive Manufacturing Benchmarking Artefact Following a Design-for-Metrology Approach. *Addit. Manuf.* **2020**, *32*, 100964. [CrossRef]

24. Rupal, B.S.; Ahmad, R.; Qureshi, A.J. Feature-Based Methodology for Design of Geometric Benchmark Test Artifacts for Additive Manufacturing Processes. *Procedia CIRP* **2018**, *70*, 84–89. [CrossRef]

25. Rupal, B.S.; Anwer, N.; Secanell, M.; Qureshi, A.J. Geometric Tolerance and Manufacturing Assemblability Estimation of Metal Additive Manufacturing (AM) Processes. *Mater. Des.* **2020**, *194*, 108842. [CrossRef]

26. Montero, J.; Weber, S.; Petroll, C.; Brenner, S.; Bleckmann, M.; Paetzold, K.; Nedeljkovic-Groha, V. Geometrical Benchmarking of Laser Powder Bed Fusion Systems Based on Designer Needs. *Proc. Des. Soc.* **2021**, *1*, 1657–1666. [CrossRef]

27. Moshiri, M.; Candeo, S.; Carmignato, S.; Mohanty, S.; Tosello, G. Benchmarking of Laser Powder Bed Fusion Machines. *J. Manuf. Mater. Process.* **2019**, *3*, 85. [CrossRef]

28. Cappellini, C.; Borgianni, Y.; Maccioni, L.; Nezzi, C. The Effect of Process Parameters on Geometric Deviations in 3D Printing with Fused Deposition Modelling. *Int. J. Adv. Manuf. Technol.* **2022**, *122*, 1763–1803. [CrossRef]

29. Dantan, J.-Y.; Huang, Z.; Goka, E.; Homri, L.; Etienne, A.; Bonnet, N.; Rivette, M. Geometrical Variations Management for Additive Manufactured Product. *CIRP Ann.* **2017**, *66*, 161–164. [CrossRef]

30. Grgić, I.; Karakašić, M.; Glavaš, H.; Konjatić, P. Accuracy of FDM PLA Polymer 3D Printing Technology Based on Tolerance Fields. *Processes* **2023**, *11*, 2810. [CrossRef]

31. *ISO/ASTM 52902:2023*; Additive Manufacturing—Test Artifacts—Geometric Capability Assessment of Additive Manufacturing Systems. International Organization for Standardization: Geneva, Switzerland, 2023.

32. Leach, R.; Carmignato, S. (Eds.) *Precision Metal Additive Manufacturing*, 1st ed.; CRC Press: Boca Raton, FL, USA, 2020; ISBN 9780429436543.

33. Ultrafuse Metal Filaments User Guidelines for 3D Printing Metal Parts. Available online: https://forward-am.com/wp-content/uploads/2021/04/UserGuidelines_2021_03_29.pdf (accessed on 14 February 2024).